Journal of Mines, Metals and Fuels, *71(10): 1483-1491; 2023. DOI: 10.18311/jmmf/2023/35814*

Print ISSN : 0022-2755

Journal of Mines, Metals and Fuels

Contents available at: *www.informaticsjournals.com/index.php/jmmf*

Influence of Thermal Slip and Ohmic Dissipation Effects on Particulate Suspension Flow through a Channel with Non-Parallel Walls

S. Ram Prasad*, S. H. C. V. Subba Bhatta and Y. S. Kalyan Chakravarthy

Department of Mathematics, M. S. Ramaiah Institute of Technology, Bangalore – 560054, India; sadhurp@gmail.com, shcvsb@gmail.com, yschakri@gmail.com.

Abstract

The main theme of this paper is a numerical investigation of fluid-particle flow in a channel with aslant walls (divergent channel) by taking thermal slip and Ohmic heating into account. The shooting technique with the RK-4 method is exploited to solve the system of dimensionless equations. Graphical discussions of the effects of emerging factors have been conducted for both fluid and particle aspects of temperature and velocity profiles. A perfect match is found when the current results are compared to the previous ones. The results reveal that the fluid phase temperature diminishes but particle phase temperature improves with an augmentation of the thermal slip parameter. These types of flows are used by a variety of industries, including the processing of waste water, mines, petrochemical sectors.

Keywords: *Divergent Channel, Joule Heating, Particulate Suspension, Thermal Slip, Two-Phase Flows*

1.0 Introduction

The flow between aslant walled channels lured innumerable investigators owing to abundant applications in various fields like bio-medicine, agriculture, engineering etc. Terrill[1] succeeded in obtaining an exact solution to analyze the flow between lopsided walls. Yilmaz *et al.*[2] have done considerable study on oblique walled channel. Motsa *et al.*[3] explored an exact solution for flow in non-symmetric boundary. Esmaeipour *et al.*[4] adopted the homotopy perturbation technique to discuss the flow in an unsymmetrical cchannel. Nazim *et al.*[5] investigated experimentally as well as numerically to study the thermal flow characteristics. Mallikarjuna *et al.*[6] numerically studied the flow in an inclined channel. Biswal *et al.*[7] deliberated numerically the nano fluid flow through channel by considering stretching and shrinking.

In gas and coal-fired power plants, the idea of two-phase flows is used to generate steam, which is extremely beneficial for turbines. Solid-liquid two-phase flows in a pipeline can be seen to be lifted in deep sea mining. Solid-particle-containing fluids are widely used in a variety of industries, including mining, chemical, and engineering. Solid-liquid flows are used in various sectors to remove material from surfaces that have been impacted by solid particles being carried by fluid. Particulate flows are one kind of two-phase flows. Particulate flows through non-uniform channels perceptible in powder manufacturing technology, waste water management, paper manufacturing etc. Ramprasad *et al.*[8] investigated how a magnetic field affected particle mobility. Sadia *et al.*[9] deliberated the radiation effect on non-uniform surface. Hady *et al.*[10] have explained convection effect on irregular boundary. Ponalagusamy and Ramakrishna[11] performed

*Author for correspondence

a numerical exploration on suspended particles in the blood. Hosam and Mahdy[12] implemented the finite difference method to discuss flow of fluid in a cone. Mallikarjuna *et al.*[13] explored numerically fluid flow in a split channel. Arshad *et al.*[14] studied analytically two-phase flow in annuli. By taking into account different pressure gradients, Rajesh Kumar *et al.*[15] studied two-phase flows through channels.

The effect of the slip near boundaries have copious applications like reducing the friction, polishing heart valves, etc. Ramprasad *et al.*[16] obtained a numerical solution to explain the slip effects on non-uniform channels. Mallikarjuna *et al.*[17] succinctly explained the particulate flow in a divergent channel. Ohmic heating has several applications in food sector and distillation of water etc. Beg *et al.*[18] studied the slip effects on nanofluid flow in a non-uniform channel. Swain *et al.*[19] concisely explained ohmic heating impact on a sheet. Umair *et al.*[20] have obtained a numerical solution for nanofluid flow in an unsymmetric channel by considering joule heating. To analyse the impacts of heat transmission in a non-uniform channel Asha and Namrata[21] used the homotopy perturbation Sumudu transformation.

The research reviewed above makes it rather evident that nobody else has tried to investigate the flow of particles in a channel with irregular walls while accounting for joule heating and slip effects. The current investigation's focus is on the effects of thermal slip and ohmic heating on the flow via unsymmetric divergent channel. With the use of a shooting technique, the RK-4 method yields a numerical solution. Graphical analysis of the effects of relevant parameters on the velocity and heat profiles for the two phases. The current results have capacious applications in various fields such as industrial metal casting, powder technology etc.

2.0 Problem Formulation

This model describes a viscous, continuous, incompressible hydromagnetic particles suspended in a fluid through an asymmetric diverging channel. The location of the channel walls is depicted in Figure 1. Variable suction/injection velocities are anticipated at various walls. The channel walls' temperature Tw is maintained at a constant level. A strong magnetic field H_0 is applied normal to the walls. In addition to this the first order temperature slip and ohmic heating are considered. The equations the governing the flow are [8,13]

Fluid phase

$$\frac{\partial}{\partial r}\left(r\overline{U}\right)+\frac{\partial \overline{V}}{\partial \theta}=0 \tag{1}$$

$$\rho\left(\overline{U}\frac{\partial \overline{U}}{\partial r}+\frac{\overline{V}}{r}\frac{\partial \overline{U}}{\partial \theta}-\frac{\overline{V}^2}{r}\right)=-\frac{\partial p}{\partial r}+\mu\left[\left(\frac{\partial^2 \overline{U}}{\partial r^2}+\frac{1}{r}\frac{\partial \overline{U}}{\partial r}+\frac{1}{r^2}\frac{\partial^2 \overline{U}}{\partial \theta^2}\right)-\frac{\overline{U}}{r^2}+\frac{2}{r^2}\frac{\partial \overline{V}}{\partial \theta}\right]+\frac{\rho_p}{\rho}S(\overline{U}_p-\overline{U})-\sigma {H_0}^2{\mu_e}^2\overline{U} \tag{2}$$

$$\rho\left(\overline{U}\frac{\partial \overline{V}}{\partial r}+\frac{\overline{V}}{r}\frac{\partial \overline{V}}{\partial \theta}-\frac{\overline{U}\overline{V}}{r}\right)=\frac{-1}{r}\frac{\partial p}{\partial \theta}+\mu\left[\left(\frac{\partial^2 \overline{V}}{\partial r^2}+\frac{1}{r}\frac{\partial \overline{V}}{\partial r}+\frac{1}{r^2}\frac{\partial^2 \overline{V}}{\partial \theta^2}\right)-\frac{\overline{V}}{r^2}+\frac{2}{r^2}\frac{\partial \overline{U}}{\partial \theta}\right]+\frac{\rho_p}{\rho}S(\overline{V}_p-\overline{V}) \tag{3}$$

$$\rho c_p\left(\overline{U}\frac{\partial T_1}{\partial r}+\frac{\overline{V}}{r}\frac{\partial T_1}{\partial \theta}\right)=k\left[\frac{1}{r}\frac{\partial}{\partial r}\left(r\frac{\partial T_1}{\partial r}\right)+\frac{1}{r^2}\frac{\partial^2 T_1}{\partial \theta^2}\right]+Q_0T_1+\frac{\rho_p c_m}{\tau_T}(T_{1p}-T_1)+\sigma {H_0}^2{\mu_e}^2\overline{U}^2 \tag{4}$$

Particle phase

$$\frac{\partial}{\partial r}(r\overline{U}_p)+\frac{\partial}{\partial \theta}(\overline{V}_p)=0 \tag{5}$$

$$\overline{U}_p\frac{\partial \overline{U}_p}{\partial r}+\frac{\overline{V}_p}{r}\frac{\partial \overline{U}_p}{\partial \theta}-\frac{{\overline{V}_p}^2}{r}=\frac{-1}{\rho_p}\frac{\partial p}{\partial r}+S(\overline{U}-\overline{U}_p) \tag{6}$$

$$\overline{U}_p\frac{\partial \overline{V}_p}{\partial r}+\frac{\overline{V}_p}{r}\frac{\partial \overline{V}_p}{\partial r}+\frac{\overline{U}_p\overline{V}_p}{r}=\frac{-1}{\rho_p}\frac{\partial p}{\partial \theta}+S(\overline{V}-\overline{V}_p) \tag{7}$$

$$\overline{U}_p\frac{\partial T_P}{\partial r}+\frac{\overline{V}_p}{r}\frac{\partial T_p}{\partial \theta}=\frac{1}{\tau_T}(T_1-T_{1p}) \tag{8}$$

The boundary conditions are

$$\overline{U}=0,\overline{U}_p=0 \text{ at } \theta=\pm\alpha,\ \overline{U}(r_0,0)=u_0$$
$$T_1=T_w-t1\frac{\partial T_1}{\partial \theta},T_{1p}=T_{wp} \text{ at } \theta=\pm\alpha \tag{9}$$

Non dimensional equations are

$$f''' + 2\,\mathrm{Re}\,ff' - f'' + L\beta(F' - f') + \left(4 - M^2\right)f' = 0 \quad \textbf{(10)}$$

$$F'' - 2\frac{\mathrm{Re}}{R}FF' - \frac{\beta}{R}(f' - F') = 0 \quad \textbf{(11)}$$

$$t'' - R\,\mathrm{Pr}\,t' + \mathrm{Pr}\,Qt + L\beta_t\gamma\,\mathrm{Pr}(T - t) + \mathrm{Pr}\,M^2 f^2 = 0 \quad \textbf{(12)}$$

$$T' - K(t - T) = 0 \quad \textbf{(13)}$$

Associated boundary conditions are

$$f(0) = 1,\ F(\pm\alpha) = 0,\ t(\pm\alpha) = 1 - \delta t'(\pm\alpha),\ T(\pm\alpha) = 1 \quad \textbf{(14)}$$

Skin friction Coefficient and Nusselt Number

$$\text{Skin friction} = C_f = \frac{\tau_s}{\rho\bar{U}_0^{\,2}} = \frac{\mu\left(\frac{\partial\bar{U}}{r\partial\theta}\right)_{\theta=\pm\alpha}}{\rho\bar{U}_0^{\,2}};$$

$$\text{Nusselt number} = Nu = \frac{rq_s}{kT_W} = \frac{r\left(\frac{-k\partial T_1}{r\partial\theta}\right)_{\theta=\pm\alpha}}{kT_W}$$

In non-dimensional form

$$C_f = \frac{1}{\mathrm{Re}}f'(\pm\alpha) \text{ and } Nu = -t'(\pm\alpha)$$

3.0 Results and Discussion

This section has covered the impact of new parameters on both temperature and velocity patterns along with particle phases. The equations (10)-(13) are solved by the shooting method. For computations the fixed values are, M=0.5, L=0.5, Re=0.5, R=0.5, Pr =0.71, Q=0.5, $\alpha = \frac{\pi}{6}$, $\delta = 0.5$ .It is articulate from Figure 2(a) that the velocity of fluid improves with the escalating values of M. As M rises, the particulate velocity lowers in the right portion of the channel and increases in the counterpart, as seen in Figure 2(b). This indicates that dominance of Lorentz force is observed in the right part. It is verified by 3(a) that the fluid's temperature goes up on the channel's right side while declining on its left. Figure 3(b) demonstrates that as M augments the particle temperature drastically shoots up. As R increases, the fluid temperature trends upward in the right part and downward in the counter part as depicted in Figure 4(a). Whereas for the particle case, complete opposite trend is noted as elucidated in the Figure 4(b). Figure 5(a) is plotted to scrutinize the impact of R on temperature of the fluid. As R augments an enhancement in temperature is noted. But an opposite trend is noticed for the particle temperature, as sketched in the Figure 5(b). It can be seen from Figure 6(a) that tends to be an increase in the velocity owing to an intensification in the values of Re in the right side, which indicates the ascendancy of inertial forces. But in the left part, the dominance of viscous force is observed. From Figure 6(b) one can confirm that an augment in Re gives to a decrement in particle velocity. Plotting Figure 7(a) allows one to see how slip affects fluid temperature. As δ augments the fluid temperature drops in the entire channel. But particle temperature boosts up for particle temperature, as depicted in Figure 7(b). It is obvious from Figure 8(a) that as Pr improves, the fluid temperature inclines in right half and declines in the left half. It indicates the domination of momentum diffusivity on the right part. Figure 8(b) demonstrates a pronounced incline in particle temperature with mounting values of Pr. Figure 9(a) is prepared to portray the impact of Q on fluid's temperature. As Q improves, the t fluid temperature augments in the right part and diminishes in the left part. It is conspicuous from Figure 9(b) the particle temperature profile gets enhanced with the improved values of Q.

The influence of sundry parameters on skin friction and Nusselt number is exhibited in Tables 2 and 3. C_f drops on both walls with an increment in R. As L, M augment, C_f shoot up on the left boundary, but they decline on the right boundary. Nu is reduced at the left boundary and improved at the right boundary with an increase in Q, Pr, M, α and δ.

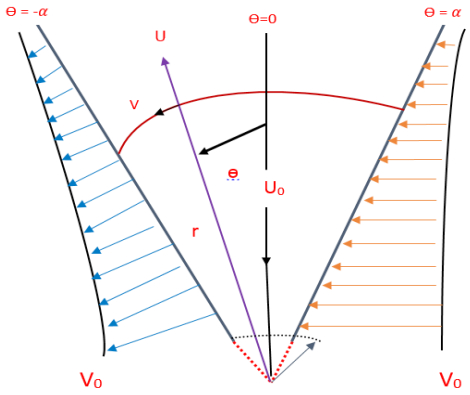

Figure 1. Flow diagram.

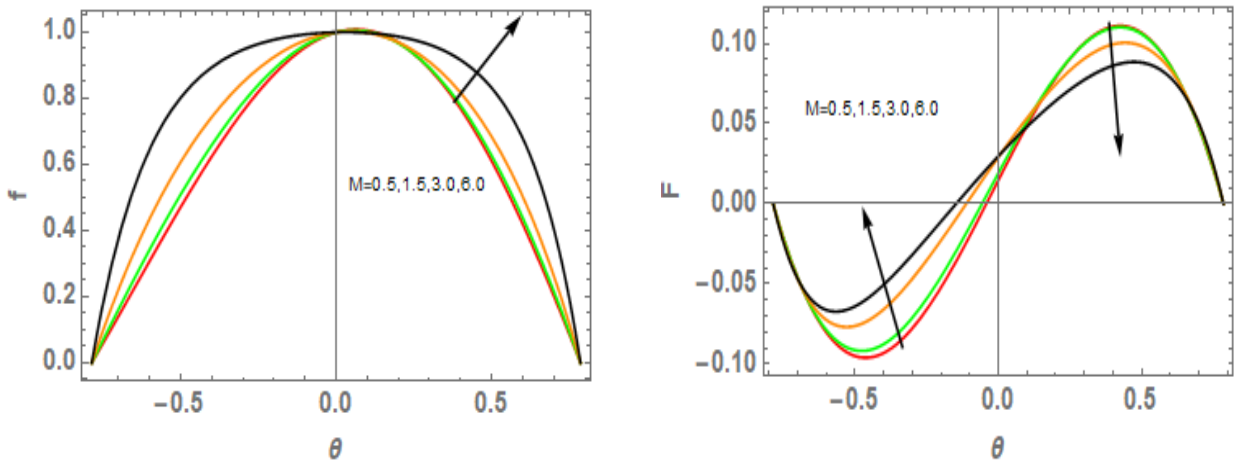

Figure 2. a). Assesment of M on *f*, b). Assesment of M on *F*

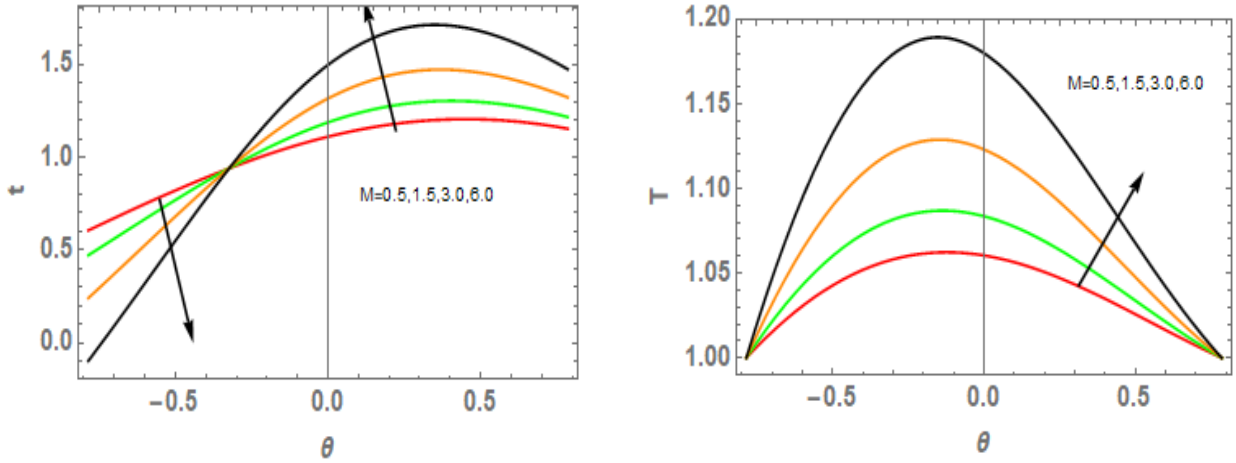

Figure 3. a). Assesment of M on *t*, b). Assesment of M on *T*

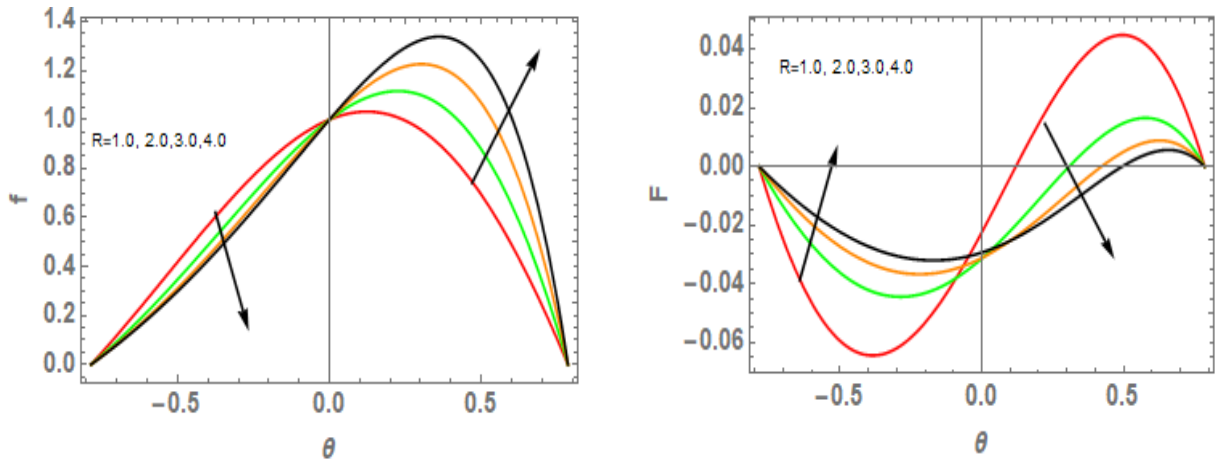

Figure 4. a). Assesment of R on *f*, b). Assesment of R on *F*

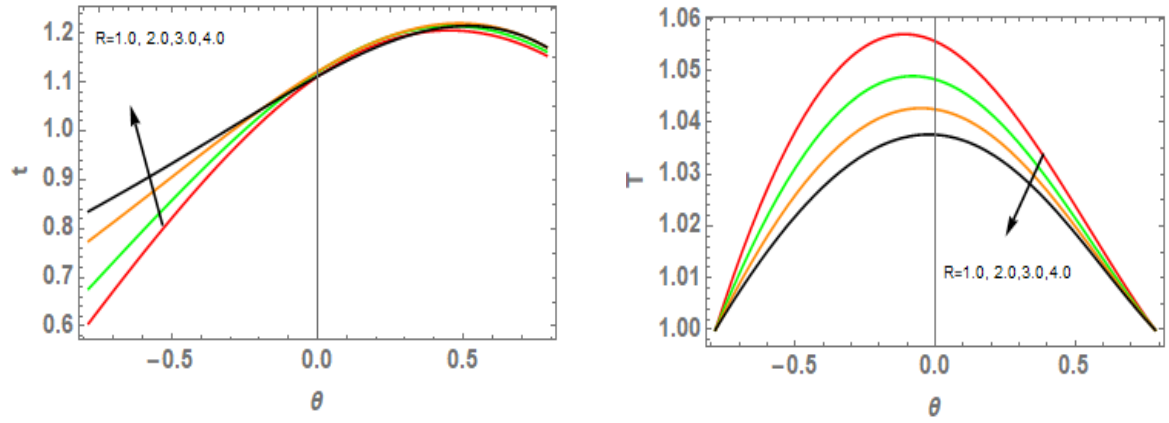

Figure 5. a). Assesment of R on *t*, b). Assesment of R on *T*

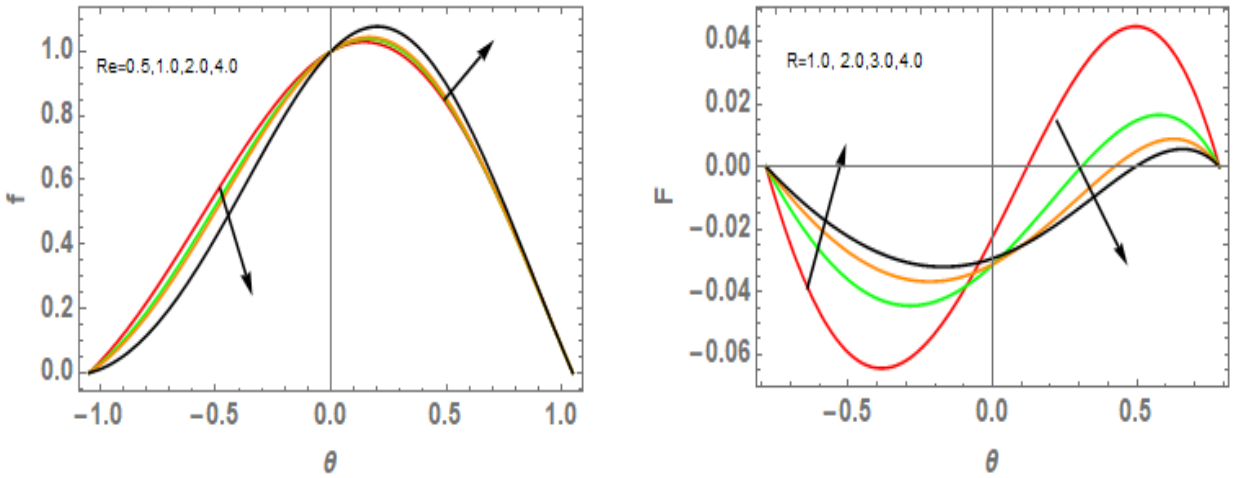

Figure 6. a). Assesment of Re on *f*, b). Assesment of R on *F*

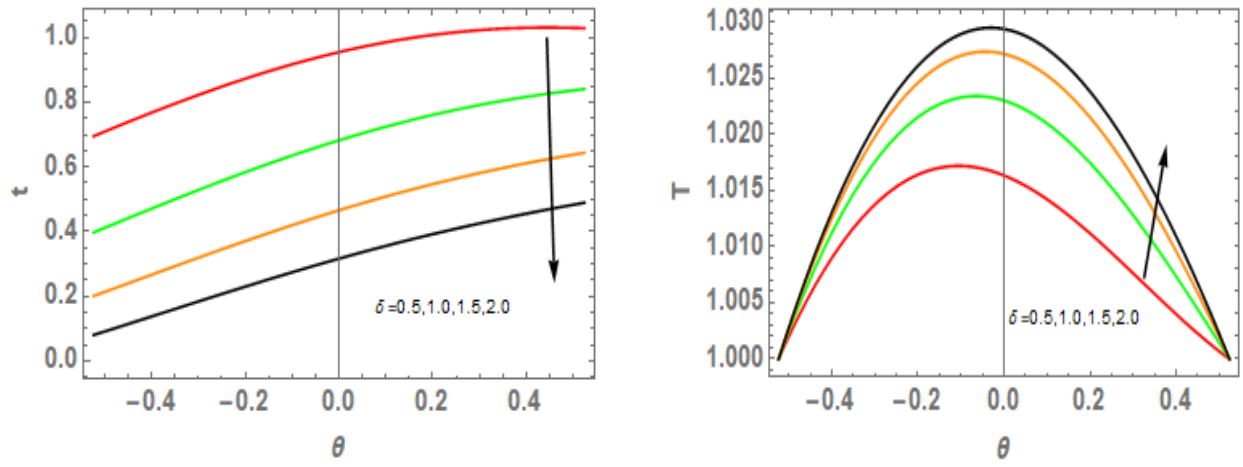

Figure 7. a). Assesment of δ on *t*, b). Assesment of δ on *T*

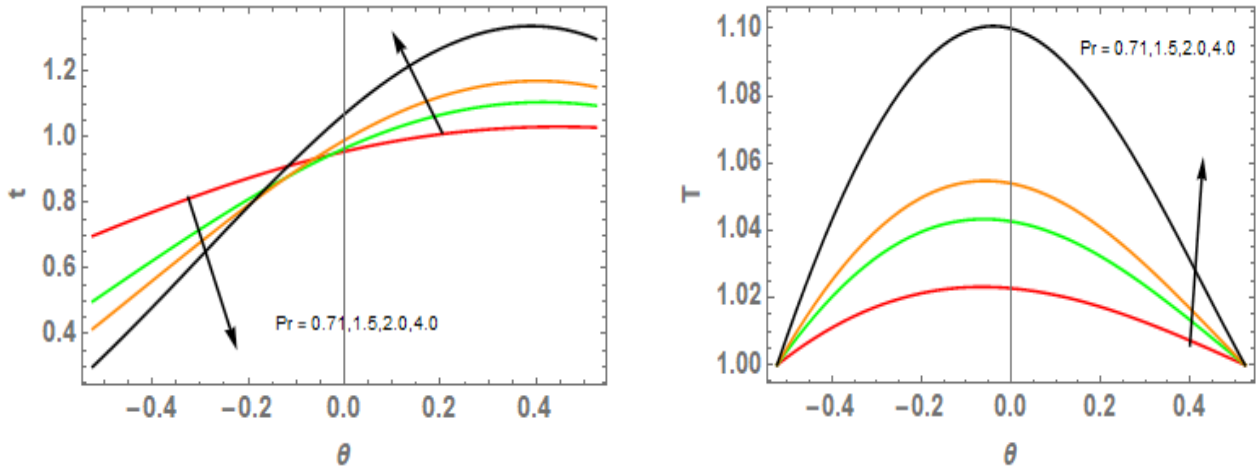

Figure 8. a). Assesment of Pr δ on *t*, b). Assesment of Pr on *T*

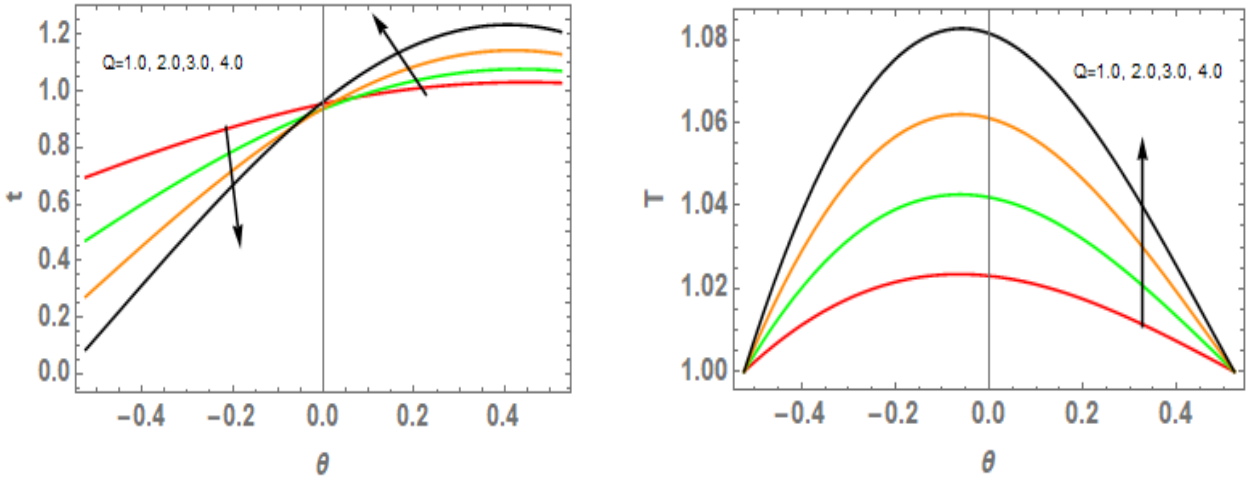

Figure 9. a). Assesment of Q δ on *t*, b). Assesment of Q on *T*

Table 1. Comparison results of skin friction coefficient for M=0, N=0, Gr=0, Pr=0, $\delta = 0$, $\beta = 1, \beta_t = 0$ k=0 and $\alpha = \frac{\pi}{6}$.

R	Re	Ramprasad *et al.*[8]		Present Results	
		c_f *at* $-\alpha$	c_f *at* α	c_f *at* $-\alpha$	c_f *at* α
1	1	2.78145	-4.22198	2.78011	-4.21994
	3	2.54596	-4.04939	2.54367	-4.00012

Table 2. Skin friction and Nusselt number for various values of R, Re, M and L

R	Re	M	L	$c_f\ at-\alpha$	$c_f\ at\ \alpha$	$Nu\ at-\alpha$	$Nu\ at\ \alpha$
0.5	0.5	0.5	0.5	3.12674	-3.84486	-0.61638	0.05659
1.0				2.84768	-4.27716	-0.52353	0.07093
1.5				2.61100	-4.76503	-0.45056	0.08219
2.0				2.41384	-5.30823	-0.39199	0.09105
	1.0			3.07026	-3.79534	-0.61600	0.05659
	2.0			2.95664	-3.69662	-0.61525	0.05657
	3.0			2.84211	-3.54848	-0.61449	0.05657
		1.5		3.31573	-4.01038	-1.18867	0.12626
		3.0		3.47724	-4.15405	-1.70243	0.18742
		6.0		3.92105	-4.55746	-3.23317	0.36376
			1	3.14323	-3.86426	-0.62337	0.05479
			1.5	3.16381	-3.88845	-0.63244	0.05252
			2	3.18436	-3.91257	-0.64190	0.05024

Table 3. Skin friction and Nusselt number for various values of α ,Q, Pr and δ

δ	Q	Pr	α	$c_f\ at-\alpha$	$c_f\ at\ \alpha$	$Nu\ at-\alpha$	$Nu\ at\ \alpha$
0.5	0.5	0.71	$\frac{\pi}{6}$	3.122621	-3.84000	-0.41472	0.11695
1.0				3.122621	-3.84000	-0.42081	0.19410
1.5				3.122621	-3.84000	-0.40413	0.22985
2.0				3.122621	-3.84000	-0.40021	0.27654
	1.0			3.122621	-3.84000	-0.35983	0.02760
	1.5			3.122621	-3.84000	-0.84748	0.09449
	2.0			3.122621	-3.84000	-1.06343	0.14004
		1.5		3.122621	-3.84000	-0.60861	0.08544
		2.0		3.122621	-3.84000	-0.71624	0.13238
		3.0		3.122621	-3.84000	-0.85908	0.24339

Table 3 Continued

			$\frac{\pi}{5}$	2.40354	-3.14869	-0.39429	0.07560
			$\frac{\pi}{4}$	1.63272	-2.44096	-0.44598	0.15345
			$\frac{\pi}{3}$	0.72265	-1.75555	-0.53416	0.30515

4.0 Conclusions

The current investigation's focus is on the effects of thermal slip and ohmic heating on the flow of particulates via slanted diverging channel with the aid of the shooting method. Principle findings are

- When M increases, the particle temperature and fluid velocity both climb, while the velocity of the particles declines in the right half of the channel and improves in the left.
- The fluid temperature falls as the thermal slip parameter rises, but the particle temperature surged.
- The fluid temperature in the left portion of the channel declines as Pr rises, whereas it rises in the right. The magnification in Pr, however, causes the particle temperature to increase.
- Heat transfer rate is high near the right boundary for improved values of Q, Pr, M, α and δ.

5.0 References

1. Terril RM. Slow Laminar Flow in a Converging or Diverging Channel with Suction at One Wall and Blowing at the Other Wall. ZAMP. 1965; 16:306.
2. Yilmaz AA, Erol S. Slow flow of a Reiner-Rivlin fluid in a converging or diverging channel with suction and injection. Turk J Eng Environ Sci. 1998; 27:179-183.
3. Motsa SS, Sibanda P, Marewo GT, Stanford Shateyi. A note on improved Homotopy Analysis Method for solving Jeffery-Hamel flow. Math Probl Eng. 2010; 359297.
4. Esmaeilpour, Naeem Roshan, Negar Roshan, Ganji DD. Analytical method in solving flow of viscoelastic fluid in a porous converging channel. Int J Math Math Sci. 2011;257903.
5. Nazim K, Harun Z, Besir Shin. Heat transfer and flow characteristics in a sinusoidally curved converging and diverging channel. Int J Therm Sci. 2020; 48:106163.
6. Mallikarjuna B, Ramprasad S, Shezahad S, Ayyaz R. Numerical and regression analysis of Cu nanoparticles flows in distinct base fluids through a symmetric non-uniform channel. Eur Phys J Spec Top. 2022; 231:557-569.
7. Uddhab B, Chakraverty S, Ojha BK, Ahmed KH. Numerical investigation on nanofluid between two inclined stretchable walls optimal Homotopy analysis method. J Comput Sci. 2022; 63:101759.
8. Ramprasad S, Subba Bhatta SHCV, Mallikarjuna B, Srinivasacharya D. Two-phase particulate suspension flow in convergent and divergent channels: A Numerical Model. Int J Appl Comput Math. 2017; 3:843-858.
9. Siddiqa S, Begum N, Hossain A, Shoabia M, Subba Reddy RS. Radiative heat transfer analysis of non-Newtonian dusty Casson fluid along a complex wavy surface. Numer Heat Transf A. 2018; 73:209-221.
10. Hady FM, Mahdy A, Mohammed SE, Omoma A, Abo Zaid. Unsteady natural convection flow of a dusty non-Newtonian Casson fluid along a vertical wavy plate: Numerical approach. J Braz Soc Mech Sci Eng. 2019; 41:472.
11. Ponalagusamy, Ramakrishna. Particle-fluid two phase modelling of electro-magneto hydrodynamic pulsatile flow of Jeffery fluid in a constricted tube under periodic body acceleration. Eur J Mech B Fluids. 2020; 81:76-92.
12. Nabwey HA, Mahdy. Numerical approach of micropolar dust-particles natural convection fluid flow due to a permeable cone with nonlinear temperature. Alexandria Eng J. 2021; 60:1739-1749.

13. Mallikarjuna B, Subba Bhatta SHCV, Ramprasad S. Velocity and thermal effects on MHD convective radiative two-phase flows in an asymmetric non-uniform channel. Propuls Power Res. 2021; 10:169-179.
14. Riaz A, Illah A, Hussain S, Ullah S, Ali K. Effects of solid particles on fluid-particulate phase flow of non-Newtonian fluid through eccentric annuli having thin peristaltic walls. J Therm Anal Calorim. 2022; 147:1645-1656.
15. Chandrawat RK, Joshi V, Beg OA. Numerical study of time-dependent flow of immiscible Saffman dusty (fluid-particle suspension) and Eringen micropolar fluids in a duct with a modified cubic B-spline Differential Quadrature method. Int Commun Heat Mass Transf. 2022; 130:105758.
16. Ramprasad S, Subba Bhatta SHCV, Mallikarjuna B. Slip effects on MHD convective Two-phase flow in a divergent channel. Defect Diffus Forum. 2018; 388:303-316.
17. Mallikarjuna B, Subba Bhatta SHCV, Ramprasad S. Velocity and thermal slip effects on MHD convective radiative two-phase flows in an asymmetric non-uniform channel. Propuls Power Res. 2021; 10:169-179.
18. Beg AO, Beg T, Khan WA, Uddin MJ. Multiple slip effects on nanofluid dissipative flow in a converging/diverging channel: A numerical study. Heat Transf. 2022; 51:1040-1061.
19. Swain BK, Parida BC, Kar S, Senapati N. Viscous dissipation and joule heating effect on MHD flow and heat transfer past a stretching sheet embedded in a porous medium. Heliyon. 2020; 6:e05338.
20. Rashid U, Iqbal A, Liang H, Khan W, Waqar M. Dynamics of water conveying zinc oxide through divergent-convergent channels with the effect of nanoparticles shape when Joule dissipation is significant. PLoS ONE. 2021;16.
21. Kotnurkar A, Kallolikar N. Effect of Joule heating and entropy generation on multi-slip condition of peristaltic flow of Casson nanofluid in an asymmetric channel. J Biol Phys. 2022; 48:273293.